Available online at www.sciencedirect.com
ScienceDirect
Optics Communications 281 (2008) 1679–1685
OPTICS COMMUNICATIONS
www.elsevier.com/locate/optcom

An all-fiber frequency-shifted feedback laser for optical ranging; signal variation with distance

V.V. Ogurtsov [a], V.M. Khodakovskyy [a], L.P. Yatsenko [a], B.W. Shore [b,*], G. Bonnet [b], K. Bergmann [b]

[a] *Institute of Physics, Ukrainian Academy of Sciences, Prospect Nauki 46, Kiev-39, 03650, Ukraine*
[b] *Technische Universität Kaiserslautern, 67653 Kaiserslautern, Germany*

Received 14 November 2007; accepted 17 November 2007

EXHIBIT A

Abstract

A recent paper [L.P. Yatsenko et al., Opt. Commun. 242 (2004) 581] provided a first-principles prediction for the optical ranging signals obtained when using a frequency-shifted feedback (FSF) laser system, seeded by a phase-modulated laser. Such a system has many useful advantages over other alternative FSF laser techniques. We report here experimental verification of that theory, specifically the variation of the amplitude modulation signal with both distance and modulation index of the seed laser. We describe the operation of an all-fiber FSF laser that uses an Er^{3+}-doped active fiber as the gain medium. To improve the signal and minimize the noise we seed the FSF laser with a phase-modulated (PM) laser; the measurement of distance derives from a measurement of amplitude modulation within a narrow frequency interval. We demonstrate that the resulting system is capable of fast and precise measurements. With the bandwidth limitations of our current system we achieved an accuracy better than 0.1 mm. Although measurements based on interferometry offer the potential for much greater accuracy under carefully controlled conditions, the present method does not suffer from the presence of a material-dependent phase shift at the surface of the measured object.

PACS: 42.55.–f; 42.60.Da; 42.55.Ah

Keywords: Lasers; Laser ranging; Frequency-shifted feedback

1. Introduction

A frequency-shifted feedback (FSF) laser is a special type of laser with a frequency shifter inside the cavity (it can be an acousto-optic modulator (AOM), a moving diffractive grating, etc.) [1–9]. The presence of such an element that shifts radiation frequency by a fixed value during each cavity round trip provides FSF lasers with several unusual properties not found with ordinary lasers. Most notably, the spectrum of a FSF laser has no well-defined longitudinal modes because the frequency shifter destroys the constructive interference inside the cavity. This makes a FSF laser a potential source of wideband continuous radiation, a property that has already found many applications [10–14]. Another important feature of a FSF laser is that, because of periodic frequency shifting on each round trip, the output radiation can be regarded as frequency swept (chirped) [6,15]. After passing through a Michelson interferometer any chirped laser will produce an amplitude modulation at a frequency proportional to the difference in length of the two interferometer arms. This makes the FSF laser a promising tool for optical ranging of distances up to several kilometers [16,17].

As describe earlier [24], optical ranging with a FSF laser can be greatly improved by using an external phase-modulated monochromatic laser to seed the FSF laser, thereby

* Corresponding author. Tel.: +1 925 455 0627.
E-mail address: bwshore@alum.mit.edu (B.W. Shore).

0030-4018/$ - see front matter © 2007 Elsevier B.V. All rights reserved.
doi:10.1016/j.optcom.2007.11.074

improving the signal detection and lessening the noise. This method was demonstrated experimentally [18] with an accuracy better than 10 μm.

Ranging devices based on all-fiber FSF lasers hold promise for practical application because of their robust and compact construction. The use of an Er^{3+}-doped active fiber as a gain medium offers particular advantages because their central wavelength, 1.55 μm, is used in telecommunication and therefore there are many readily available inexpensive fiber elements and devices for that wavelength. Another advantage of erbium lasers, very important for any industrial application, is their safety for eyes.

Our technique, like those based on interferometry, has at first glance an intrinsic ambiguity regarding the deduction of a length from a time or frequency: the measurements only give a result modulo an increment. Interferometric methods commonly use the technique of an effective wavelength, based on the use of two wavelengths or a phase modulation, to resolve the ambiguity. We have noted appropriate approaches to overcome this problem.

The present paper describes the experimental characteristics of an all-fiber FSF laser with Er^{3+}-doped active fiber as the gain medium. It is seeded by a phase-modulated (PM) laser for precise measurements of distances. Using this laser we are able to confirm the recent first-principles derivation [24] of the dependence of signal strength upon distance; the predicted Bessel function behavior is clearly seen.

2. Er^{3+}-doped fiber FSF laser

As shown in Fig. 1, the all-fiber FSF laser consists of a fiber cavity (optical length 19.2 m), into which is inserted an Er^{3+}-doped active fiber (5 m long) pumped by a diode laser of wavelength 980 nm) through a wavelength division multiplexer (WDM). The frequency-shifting element is an acousto-optic modulator (AOM) that upshifts the intracavity radiation by 80 MHz with each round trip. Output and seed insertion occurs through two 10% couplers. We use two couplers instead of one to avoid placing 90% of the

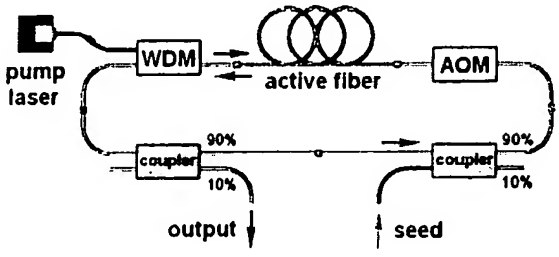

Fig. 1. Layout of the all-fiber FSF laser. Light from a pump laser enters the fiber circuit through a WDM (top left) and provides gain in an Er^{3+}-doped active fiber (shown as loops). Within the circuit the FSF light travels counterclockwise, starting from an external seed laser (lower right) entering the circuit through a coupler that transmits 10% of this light. An AOM induces a frequency upshift of 80 MHz prior to amplification in the active fiber. A second coupler diverts 10% of the light into output for observation.

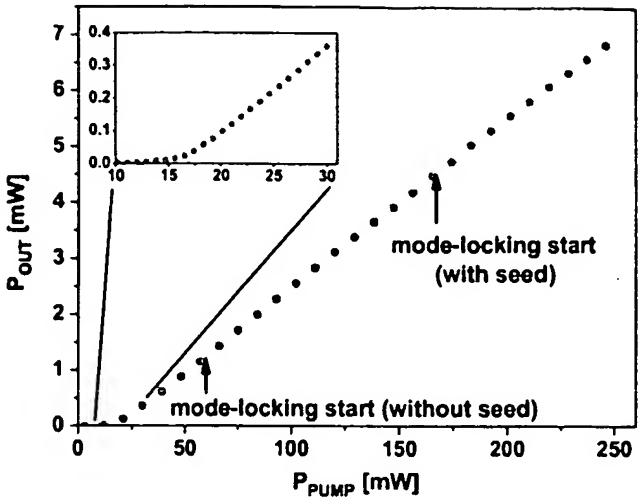

Fig. 2. Power characteristics of the all-fiber FSF laser with and without the seed laser: output power P_{out}, in mW, as a function of pump power P_{pump}, also in mW. The insert shows the threshold region. The output exhibits mode-locking, with consequent formation of pulse trains, when the pump power is sufficiently large. The arrows show the beginning of the mode-locking regime with and without external seed: the presence of the seed increases the power at which mode-locking starts. The useful regime for ranging is to the left of these arrows.

seed laser power into the output radiation [19]. All fiber components are joined by a fusion splice.

The output characteristics of our FSF laser are typical (see Fig. 2): the output power increases linearly with the pump power above a threshold of about 15 mW pump. A common feature of FSF lasers [5,19] is that for sufficiently high pump power a self mode-locking regime usually exists. Such pulse-train output is not suitable for optical ranging. In our laser, in the absence of the seed laser, mode-locking appears at quite low pump power (about 60 mW). Injection of an external CW seed greatly increases the threshold pump power for self mode-locking from about 60 mW to about 170 mW, thereby extending the CW-regime that is suitable for distance measurements [19].

The spectrum of this laser with and without external monochromatic seed is a slightly asymmetric Gaussian (Fig. 3) with FWHM 150–160 GHz. The FSF laser spectrum without a seed laser is continuous whereas with a seed it consists of equidistant components (unresolved in Fig. 3) separated by the AOM frequency [15,19,20].

3. Ranging with a FSF laser seeded by a phase-modulated external laser

The output radiation from a FSF laser can be described by a so-called "moving comb" model [15,16,20–23]. In this model a FSF laser, characterized by a round-trip time τ_r and an AOM frequency Δ, has an output spectrum comprising a very large number (103 or more) of equidistant frequencies (comb teeth), separated by the cavity axial mode interval $\Delta_c = 2\pi/\tau_r$, and moving with the rate $\gamma \equiv \Delta/\tau_r$,

$$\omega_n(t) = \omega_{max} + \gamma t - n\Delta_c. \quad (1)$$

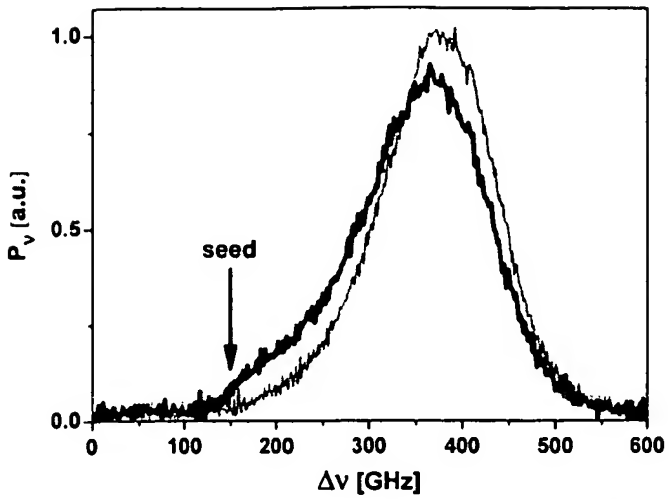

Fig. 3. Spectrum of the all-fiber FSF laser with (thick black line) and without (thin red line) the external seed laser. The arrow marks the frequency of the seed laser. The presence of the seed introduces some distortion of the spectrum, but it remains reasonably well-described by a Gaussian. (For interpretation of the references to color in this figure legend, the reader is referred to the web version of this article.)

Here, as in previous work, the constant ω_{max} is the frequency at which the time varying component has maximum amplitude. Fig. 4aa portrays, at a fixed time t, this frequency comb. Such a field, when delayed by time increment T, will again appear as a frequency comb, but offset (at time t) by a frequency increment γT (see Fig. 4b).

For application to ranging these two fields are those of the two arms of a Michelson interferometer whose arms differ in length by L. The resulting time delay $T = 2L/c$ produces a set of difference frequencies, from combinations

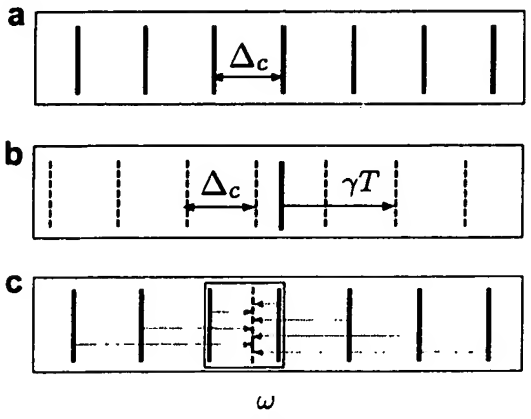

Fig. 4. (a) A portion of the sequence of equidistant discrete FSF-output frequencies (solid vertical lines) at a fixed time t, separated by the cavity-mode spacing Δ_c. (b) The output frequencies (dashed vertical lines) after the field undergoes a delay in time, as would occur with a reflected field. Shown is one possible value of γT that would produce this sequence, along with a single unshifted component (solid line); other possibilities differ by $n\Delta_c$, with integer n. (c) Arrows mark some of the frequency differences that are beat-frequency signals, observable as resonances. Those pointing to the right contribute to the "direct" resonances, those to the left contribute to the "reverse" resonances. The central rectangle encloses a frequency interval of size Δ_c used for measurement.

of different teeth of the reference and reflected fields. Fig. 4c shows some of these frequencies. Two classes occur, distinguished in the figure by arrows pointing to the right and arrows pointing to the left. These frequency differences are observed as beat signals at the frequencies

$$\omega_B^+(q) = q\Delta_c + \gamma T \tag{2}$$

and

$$\omega_B^-(p) = p\Delta_c - \gamma T \tag{3}$$

with integer $q, p = 0, \pm 1, \pm 2, \ldots$

At each frequency $\omega_B^{\pm}(n)$ the beating signal is a sum of many contributions from paired teeth of the reference and reflected fields (each with the same frequency difference $\omega_B^{\pm}(n)$). A very important feature of a FSF laser is that in the absence of fluctuations, e.g. those caused by spontaneous emission, the phases of all these contributions are balanced in such a way that their *sum is equal to zero*. However, unavoidable fluctuations break this balance, and one can therefore observe a resonant increase in the spectral density of the RF spectrum of the Michelson interferometer output intensity fluctuations near these beat frequencies. Such signals have been used for distance measurements in [16,17]. Recently we have proposed [24] and experimentally demonstrated with a Yb^{3+}-doped fiber-ring FSF laser [18] another approach to distance measurements, based on the use of a phase-modulated laser as an external seed. When the output of such a laser passes through a Michelson interferometer, the phase modulation induces amplitude modulation. The variation of the magnitude of the amplitude modulation as a function of the modulation frequency Ω reveals very sharp resonances. This occurs whenever Ω coincides with the beat frequencies given by Eq. (2) or (3).

From a measurement of the frequency associated with the maxima of the amplitude modulation signal we can deduce the delay T and hence the distance L. Because the monochromatic amplitude modulation of the FSF laser output can be measured with a very narrow-bandwidth filter, the technique allows a significant decrease in the noise and a corresponding improvement in the signal-to-noise ratio.

Fig. 5 shows the various resonance frequencies $\omega_B^+(q)$ and $\omega_B^-(p)$ for given delay time T, and hence for distance $L = cT/2$. The locus of values appear as lines marked by integers p and q. For best results the modulation frequency should be chosen within a region convenient for measurements. The most natural choice is a modulation frequency which is smaller than the free spectral range of the cavity, Δ_c (or the cavity mode spacing)

$$0 < \Omega < \Delta_c, \tag{4}$$

shown hatched in Fig. 5. In this region, where $L \neq k\pi c/\Delta$, $(k = 0, 1, 2, \ldots)$, there exist, for a given γT, two resonance frequencies, $\Omega = \Omega_D$ and $\Omega = \Omega_R$, corresponding to specific values of integers p and q. With increasing distance L the "direct" resonance frequency Ω_D increases and the

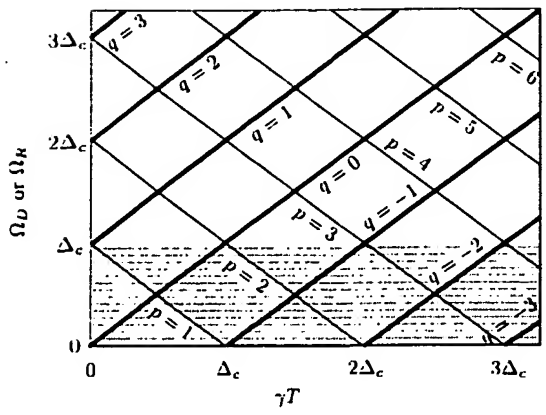

Fig. 5. Possible frequencies of amplitude modulation resonances, Ω_D or Ω_R, as functions of $\gamma T \equiv (2\Delta/c\tau_r)L$. Thick lines, labelled by q, mark values for Ω_D, Eq. (5). Thin lines, labelled by p, mark values for Ω_R, Eq. (6). The shaded portion marks the region $0 < \Omega < \Delta_c$ used for frequency modulation.

"reverse" frequency Ω_R decreases. The relevant connection with distance comes from Eq. (2) or (3), namely

$$\Omega_D = q\Delta_c + (2\Delta/c\tau_r)L \tag{5}$$

and

$$\Omega_R = p\Delta_c - (2\Delta/c\tau_r)L. \tag{6}$$

As with any interferometry, there is an ambiguity in the present technique. Distances which differ by an integer number of intervals $L_\Delta = \pi c/\Delta$ give the same resonance frequencies in the interval $0 < \Omega < \Delta_c$. This ambiguity is resolvable by measuring changes $\delta\Omega_D$ or $\delta\Omega_R$ produced by changing the AOM frequency from Δ to $\Delta + \delta\Delta$ [16,17]. The required theoretical relationship is obtained from Eqs. (5) and (6) for constant Δ_c, and with variable Δ. As long as the change $\delta\Delta$ of the AOM frequency is small enough that integers q and p do not change we obtain the distance L from the formula

$$L = \frac{c\tau_r}{2}\frac{\delta\Omega_D}{\delta\Delta} = -\frac{c\tau_r}{2}\frac{\delta\Omega_R}{\delta\Delta}. \tag{7}$$

4. Variation of amplitude modulation signal with distance

For practical applications it is important to know the degree of amplitude modulation at resonance. To derive it consider, following [24], the FSF laser seeded by a CW laser whose phase $\Phi(t) = \omega_s t + \varphi_s(t)$ is modulated sinusoidally,

$$\varphi_s(t) = \varphi_0 + \beta\sin(\Omega t). \tag{8}$$

Here ω_s is the seed laser frequency, β is the modulation index and φ_0 is the initial phase. To obtain the amplitude modulation signal we model the FSF-laser output as a discrete spectrum. In [15] we have shown that this model is equivalent to the moving comb model. In this model the FSF-laser output consists of a set of discrete optical components with the frequencies $\omega_s + n\Delta$ ($n = 0, 1, 2, \ldots$). The phases of the components have a time-independent contribution that is quadratic in n and a time-delayed contribution from the phase-modulated seed laser phase $\varphi_s(t - n\tau_r)$. The amplitudes of the components are proportional to a Gaussian function of n,

$$a_n = a_{max}\exp\left[-(n - n_{max})^2/n_w^2\right], \tag{9}$$

where n_w is the effective number of optical components within the Gaussian profile of the laser spectrum, n_{max} identifies the component closest to the maximum of the spectral profile and a_{max} is the amplitude of the central component. The parameters n_w and n_{max} are large, $n_w \gg 1$ and $n_{max} \gg 1$, and can be evaluated from measurable laser characteristics (for details see Eqs. (13)–(17) in [15]).

When this output enters a Michelson interferometer whose arms differ in length by L, the interference term in the interferometer output intensity is a sum of independent contributions $\delta P_{int}^{(n)}$ from each nth frequency component. Every contribution is proportional to a cosines of the phase difference between reference and reflected components

$$\phi_n = (\omega_s + n\Delta)T + \varphi_s(t + T - n\tau_r) - \varphi_s(t - n\tau_r) \tag{10}$$

and to the square of the component amplitude:

$$\delta P_{int}^{(n)} \propto a_n 2\cos\phi_n. \tag{11}$$

Because the phase $\varphi_s(t)$ of the seed laser is modulated, the difference phase ϕ_n will also be modulated, with a time-dependent part

$$\delta\phi_n(t) = 2\beta\sin[\Omega T/2]\cos[\Omega t + \Omega T/2 - n\Omega\tau_r], \tag{12}$$

as follows from Eq. (8) and the use of a trigonometric identity. Thus the contribution of each individual component has an amplitude modulation with the period $2\pi/\Omega$. Making use of a Jacobi–Anger expansion [25]

$$\exp[iZ\cos(\theta)] = \sum_{l=-\infty}^{\infty} i^l J_l(Z)\exp[il\theta] \tag{13}$$

one can consider this periodic modulation as a sum of the harmonic components with the frequencies $l\Omega$ ($l = 1, 2, \ldots$) and with the amplitudes proportional to the Bessel function $J_l(Z)$ of integer order l and of argument $Z = 2\beta\sin(\Omega T/2)$. The amplitude $S_n(\Omega, T)$ of the harmonic of present interest, the first harmonic, varies with time delay $T = 2L/c$ and with frequency Ω in accordance with the formula,

$$S_n(\Omega, T) = s_0 J_1(2\beta\sin[\Omega T/2])a_n 2, \tag{14}$$

where $J_1(Z)$ is the Bessel function of order 1 and s_0 is a normalization factor that incorporates the laser output power. For particular combinations of the modulation index β, the modulation frequency Ω and the time delay T, the amplitude modulation with frequency Ω may actually be suppressed for each elementary interference term. This will occur when

$$2\beta\sin[\Omega T/2] = j_{1,k}, \tag{15}$$

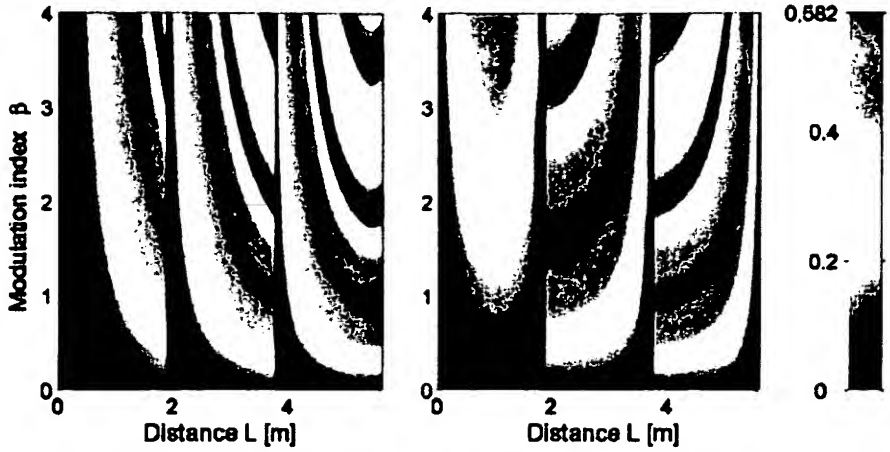

Fig. 6. Density plot of the calculated amplitude-modulation signal S_A as a function of distance L and the modulation index β. The left frame corresponds to the "direct" signal, the right frame corresponds to the "reverse" one. The basic length scale of the figure is $L_0 = \pi c/\Delta = 1.875$ m for our AOM frequency of $\Delta = 80$ MHz.

where $j_{1,k} = 0, 3.8317, 7.0156, \ldots$ are the kth zeros of the Bessel function of order 1.

If the condition (15) is not fulfilled it is easy to see from (10) and (12) that there are two sets of elementary contributions to the signal of the amplitude modulation with depending on n phases: a "direct" signal with phase $\psi_n^{(+)} = n(\Omega\tau_r + \Delta T)$ and a "reverse" signal having phase $\psi_n^{(-)} = n(\Omega\tau_r - \Delta T)$.

The sum of these contributions, weighted by the smoothly varying squared amplitude a_n^2 will be zero for all Ω except for very narrow intervals near the frequencies Ω_p providing that

$$\Omega_p\tau_r \pm \Delta T = 2\pi p \tag{16}$$

with $p = 0, \pm 1, \pm 2 \ldots$ Note that the frequencies Ω_p determined by this condition coincide with the beating frequencies of Eqs. (2) and (3) obtained from the moving comb model.

Regarded as a function of modulation frequency Ω, the amplitude modulation signal has a Gaussian profile: it has the width $\Delta\Omega = 2\sqrt{2}/(\tau_r n_w)$ and reaches a maximum

$$S_A(\Omega, T) = S_0 J_1(2\beta \sin[\Omega T/2]) \tag{17}$$

with $S_0 = n_w s_0 \sqrt{\pi/2}$, when the modulation frequency Ω has the value determined by Eq. (16). Thus by measuring the modulation frequency for which the amplitude modulation of the interferometer output maximizes, and knowing the chirp rate γ, we obtain the interferometer-arm difference L.

Fig. 6 shows a density plot of the amplitude modulation signal S_A, calculated from Eq. (17), as a function of the distance L and the modulation index β for the "direct" and "reverse" signal. The basic scale length of the interferometer-arm difference L_0 for this plot is determined by the condition $\gamma T \equiv \Delta T/\tau_r = \Delta_c$. Using the relationships $T = 2L/c$ and $\Delta_c = 2\pi/\tau_r$ we obtain $L = \pi c/\Delta$. Thus, the scale length in Fig. 6 is determined by the AOM frequency Δ. Our AOM frequency is 80 MHz, leading to the distance scale of $L_0 = \pi c/\Delta = 1.875$ m, apparent in the figure.

The Bessel function in the expression (17) for the signal produces a strong variation of the signal S_A with distance L and modulation index β. Fig. 6 illustrates this rather complicated behavior. The regions of minimal signal (dark blue[1] regions in Fig. 6) pose challenges for detection. However, these can be circumvented by proper selection of the modulation index β at each distance L.

The preceding analysis assumed a monochromatic seed. In reality the seed laser has a finite spectral width, set by the finite coherence length of the seed laser. This will decrease the signal (17) in a manner that can be approximately described by a damping factor $\exp(-L/L_{coh})$, where L_{coh} is the coherence length of the seed laser:

$$S_A = S_0 J_1(2\beta \sin[\Omega L/c]) \exp(-L/L_{coh}). \tag{18}$$

The inclusion of a finite bandwidth of the seed laser does not alter the Bessel-function variation of the signal amplitude with distance L.

5. Experimental results and comparison with theory

Fig. 7 shows the experimental setup we used for the distance measurements. It consists of an all-fiber FSF laser seeded by a phase-modulated external monochromatic diode laser. The output power of the FSF laser passes through a Michelson interferometer with one fixed and one movable arm. The distance difference between them can be changed from 15 cm to 5 m. After emerging from the Michelson interferometer the laser light impinges on a photodetector with bandwidth 50 MHz connected to a lock-in amplifier. The latter is driven by the same generator that operates the electro-optic modulator. Thus the lock-in amplifier detects resonances of the amplitude modulation S_{AM} that correspond to various distances L. We observed the spectrum of the FSF laser using a Fabry–Perot interferometer (FPI) with the free spectral range of 650 GHz, see Fig. 7.

[1] For interpretation of color in Fig. 6, the reader is referred to the web version of this article.

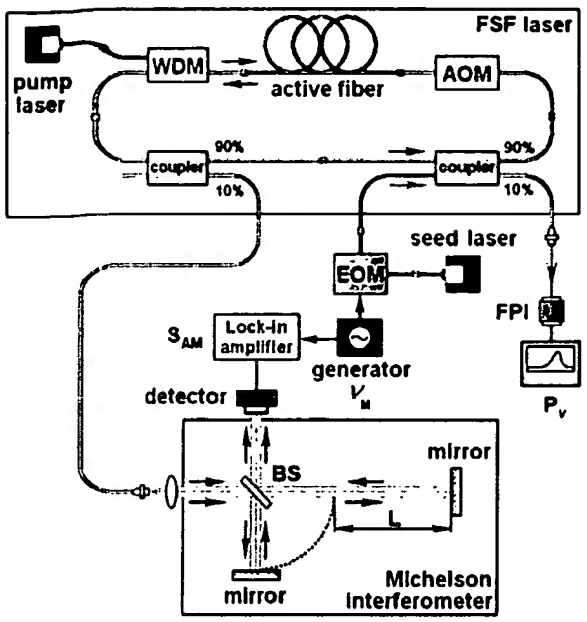

Fig. 7. Experimental setup for distance measurements. The upper rectangle encloses the FSF laser of Fig. 1. The seed laser is modulated by an EOM. The output coupler feeds 10% to the Michelson interferometer (rectangular box at bottom of the figure), one arm of which includes the length L to be measured. The output from a beam splitter (BS) in the interferometer is detected as an amplitude modulation signal S_A with a lock-in amplifier matched to the frequency of the EOM. The seed input coupler also provides output analyzed by a Fabry–Perot interfermometer (FPI).

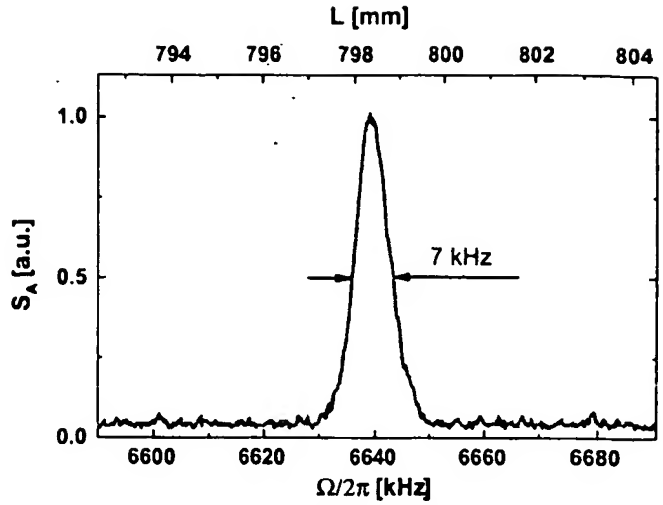

Fig. 8. Amplitude modulation signal S_A versus modulation frequency Ω.

Fig. 8 shows a typical example of a narrow "direct" resonance in the magnitude S_A as a function of the modulation frequency Ω. Because in this case the distance L is smaller than $\pi c/\Delta$ the frequency of the resonance maximum is directly proportional to L. For our laser system the proportionality constant is 8.316 kHz/mm. The FWHM of the resonance is about 7 kHz. Thus, the resolution available with our system is better than 1 mm and the accuracy is better than 0.1 mm (assuming that the frequency position of the resonance maximum can be determined within 10% of its width).

As was mentioned above, the amplitude modulation signal S_A has a complicated dependance upon the distance L and the index of modulation β, described by formula (18). Fig. 9a and b compare the experimental results with the theoretical calculation made for our laser system. The experimental results are in excellent agreement with the theory.

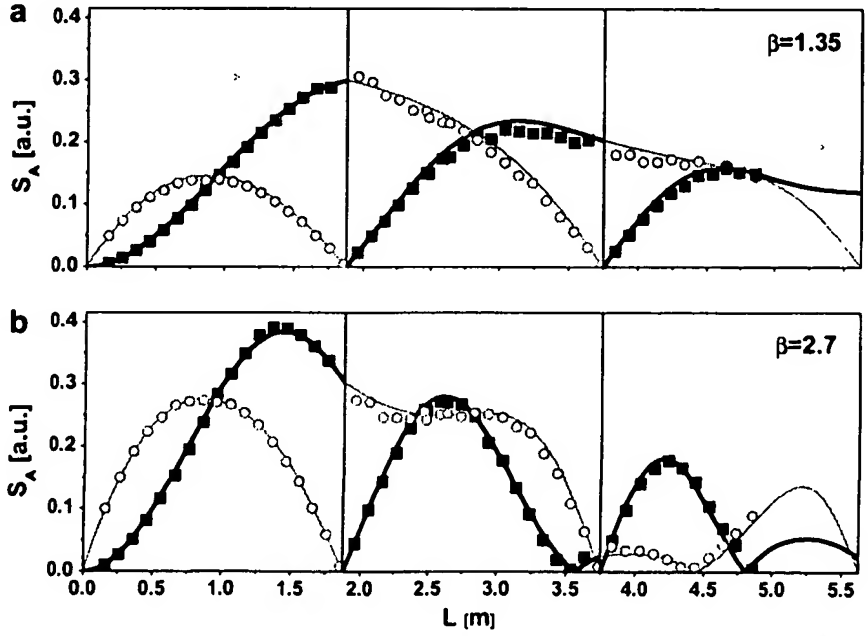

Fig. 9. Dependance of the amplitude modulation signal size upon the distance for a modulation index $\beta = 1.35$ (frame a) and $\beta = 2.7$ (frame b). Dots are experimental results and lines are theoretical simulation. Black squares and thick lines refer to the "direct" maxima (D, see Fig. 5), red circles and thin lines refer to "reverse" maxima (R).

Fig. 9 shows that there are two minima of the "direct" signal for $\beta = 2.7$, at the distances 3.6 and 4.8 m. These do not exist for $\beta = 1.35$. This means that for any distance L there is an optimal modulation index β such that it is possible to avoid signal minima. Thus the useful range of our method is limited only by the coherence length of the seed laser (this was 3.6 m in our work), which is set by the bandwidth of the seed, and the collection efficiency of the reflected light. For our setup this latter restriction is several tens of meters.

6. Summary and conclusions

This paper describes an all-fiber FSF laser with Er^{3+}-doped fiber as the gain medium and an acousto-optic modulator as the frequency shifter. The spectral and power characteristics are presented for cases with and without an external seed laser; these are typical of FSF lasers.

We have used our system, a FSF laser with an external PM seed laser, to measure distances with a Michelson interferometer scheme. We display examples of the amplitude-modulation signal for distances ranging from 15 cm to 5 m. Our results are in very good quantitative agreement with numerical simulations which take the finite bandwidth of the seed laser into account. We thereby verify the theory first presented in [24]. Notably, the signal exhibits pronounced minima at particular distances, set by the zeros of a Bessel function. These "blind" zones can be avoided by changing the modulation index of the PM seed laser and/or the AOM frequency.

The all-fiber FSF laser seeded by an external PM laser is a powerful noise-immune tool for distance measurements over a range of distances up to tens of meters. The bandwidth limitation of our present apparatus allows an accuracy better than 0.1 mm and resolution better than 1 mm.

Dual wavelength interferometric measurements offer the opportunity to determine lengths to within a small fraction of a wavelength, as numerous publications have attested [26–29]. Such high accuracy is only possible under carefully controlled conditions. However, measurements of distances to arbitrary objects require detailed information about the surface, because there occurs a material-dependent phase shift that affects any measurement based on phases, such as interferometry [30]. Techniques based on the use of a FSF laser, being essentially measurements of time rather than phase, do not suffer from this problem.

Acknowledgments

We acknowledge support by the Stiftung Rheinland-Pfalz für Innovation and by CNES, INTAS and NSAU (06-1000024-9075). L.P.Y. acknowledges support by the Deutsche Forschungsgemeinschaft (436-UKR-113/16). B.W.S. acknowledges support from the Max Planck Forschungspreis awarded to K.B. in 2003.

References

[1] L.C. Foster, M.D. Ewy, C.B. Crumly, Appl. Phys. Lett. 6 (1965) 6.
[2] W. Streifer, J.R. Whinnery, Appl. Phys. Lett. 17 (1970) 335.
[3] J. Martin, Y. Zhao, S. Balle, I.C.M. Littler, K. Bergmann, Opt. Commun. 111 (1994) 101.
[4] A.P. Willis, A.I. Ferguson, D.M. Kane, Opt. Commun. 116 (1995) 87.
[5] G. Bonnet, S. Balle, Th. Kraft, K. Bergmann, Opt. Commun. 123 (1996) 790.
[6] K. Kasahara, K. Nakamura, M. Sato, H. Ito, IEEE J. Quantum Electron. 34 (1998) 190.
[7] K.A. Shore, D.M. Kane, IEEE J. Quantum Electron. 35 (1999) 1053.
[8] J. Geng, S. Wada, Y. Urata, H. Tashiro, Opt. Lett. 24 (1999) 676.
[9] J. Geng, S. Wada, Y. Urata, H. Tashiro, Opt. Lett. 24 (1999) 1635.
[10] I.C.M. Littler, H.M. Keller, U. Gaubatz, K. Bergmann, Zs. Phys. D 18 (1991) 307.
[11] D.T. Mugglin, A.D. Streater, S. Balle, K. Bergmann, Opt. Commun. 104 (1993) 165.
[12] J.R.M. Barr, G.Y. Liang, M.W. Phillips, Opt. Lett. 18 (1993) 1010.
[13] M.J. Lim, C.I. Sukenik, T.H. Stievater, P.H. Bucksbaum, R.S. Conti, Opt. Commun. 147 (1998) 99.
[14] M. Cashen, V. Bretin, H. Metcalf, J. Opt. Soc. Am. B 17 (2000) 530.
[15] L.P. Yatsenko, B.W. Shore, K. Bergmann, Opt. Commun. 236 (2004) 183.
[16] K. Nakamura, T. Miyahara, M. Yoshida, T. Hara, H. Ito, Photon. Technol. Lett. 10 (1998) 1772.
[17] K. Nakamura, T. Hara, M. Yoshida, T. Miyahara, H. Ito, IEEE J. Quantum Electron. 36 (2000) 305.
[18] V.V. Ogurtsov, L.P. Yatsenko, V.M. Khodakovskyy, B.W. Shore, G. Bonnet, K. Bergmann, Opt. Commun. 266 (2006) 266.
[19] V.V. Ogurtsov, L.P. Yatsenko, V.M. Khodakovskyy, B.W. Shore, G. Bonnet, K. Bergmann, Opt. Commun. 266 (2006) 627.
[20] I.R. Perry, R.L. Wang, J.R.M. Barr, Opt. Commun. 109 (1994) 187.
[21] M.W. Phillips, G.Y. Liang, J.R.M. Barr, Opt. Commun. 100 (1993) 473.
[22] K. Nakamura, F. Abe, K. Kasahara, T. Hara, M. Sato, H. Ito, IEEE J. Quantum Electron. 33 (1997) 103.
[23] A. Yoshizawa, H. Tsuchida, Opt. Commun. 155 (1998) 51.
[24] L.P. Yatsenko, B.W. Shore, K. Bergmann, Opt. Commun. 242 (2004) 581.
[25] Weisstein, Eric W. Jacobi–Anger Expansion. From MathWorld–A Wolfram Web Resource. <http://mathworld.wolfram.com/Jacobi-AngerExpansion.html>.
[26] F. Bien, M. Camac, H.J. Caulfield, S. Ezekiel, Appl. Opt. 23 (1981) 2982.
[27] P. de Groot, J. McGarvey, Opt. Lett. 17 (1992) 1626.
[28] P. Hariharan, D. Malacara, B.J. Thompson (Eds.), Interference, Interferometry, and Interferometric Metrology, SPIE Optical Engineering Press, Bellingham, WA, 1995.
[29] O.P. Lay, S. Dubovitsky, R.D. Peters, J.P. Burger, S.-W. Ahn, W.H. Steier, H.R. Fetterman, Y. Chang, Opt. Lett. 28 (2003) 890.
[30] L.P. Yatsenko, M. Loeffler, B.W. Shore, K. Bergmann, Appl. Opt. 43 (2004) 3241.